Robotica (1997) volume 15, pp 645–652. Printed in the United Kingdom © 1997 Cambridge University Press

Ultrasonic classification and location of 3D room features using maximum likelihood estimation – Part II*

Mun-Li Hong** and Lindsay Kleeman†

(Received in Final Form: January 8, 1997)

SUMMARY

This paper is part II of a paper published in the previous issue of *Robotica.* This part proceeds from the assumption that 3D features have been calssified into either a plane, a 2D corner type I or II, or a 3D corner using the Maximum Likelihood Estimator. The location of the 3D features from the results of the Maximum Likelihood Estimation are derived here. Experimental results characterising the ultrasonic sensor and its application to a robot localisation problem are presented in this paper.

KEYWORDS: Ultrasonic sensors; 3D features; Maximum likelihood estimation.

INTRODUCTION

The paper is arranged in two parts. Part I is in the previous issue of Robotica and contains Sections 1 to Section 7. In part I, section 1 provides an introduction to ultrasonic robot localisation and the desirability of using 3D room features as passive beacons. The minimum number of transducers required to classify planes, 2D corners and 3D corners are derived in Section 2. Sections 3 and 4 present the sensor configuration and discussion on the degrees of freedom of the beacons. The conventions used and the theoretical derivation of the times of flight for each type of room feature are presented in Sections 5 and 6. Section 7 discusses the Maximum Likelihood Estimation and how it is used to classify the different reflectors. This paper (Part II) contains derivations of target location from the MLE classification, the results of the experimental characterisation of the sensor, discussion of robot localisation experiments, and the references. The numberings for figures, tables and equations are preceded by I or II to indicate that the figures, tables and equations are located in Part I or Part II of the paper.

1. REFLECTOR LOCALISATION

After the Maximum Likelihood estimates of the distances of flight, $\hat{r}_{11}$, $\hat{r}_{22}$ and $\hat{r}_{33}$, are obtained from $\hat{\mathbf{B}}$ in equation (I-25), the position of the reflector at this *most likely location* can be calculated using the invariance property of MLE. The following subsections derive mathematical expressions for the range and orientation of the reflector with respect to the sensor system in terms of r_{11}, r_{22} and r_{33}. The azimuth and elevation of the reflector with respect to the sensor frame are represented by the rotational angles α and β about u and v axes respectively as shown in Figure I-8.

(a) Plane

Since the result of the projection made in section 6 of part I lies on the vw plane (refer to Figure I-9), it is observed that the rotational angle α about u axis is the same as the angle θ_{11} which, from equation (I-1), is,

$$\alpha = \theta_{11} = \sin^{-1}\left(\frac{\hat{r}_{22} - \hat{r}_{11}}{2d}\right) \tag{II-1}$$

To determine the rotational angle β about the v axis, it is necessary to include the transducer $T3$ in the geometrical analysis as follows. From Figure II-1, it can be shown that

$$\beta = \sin^{-1}\left(\frac{\hat{r}_{11} - \hat{r}_{33} + d\sin\alpha}{\sqrt{3}d\cos\alpha}\right) \tag{II-2}$$

The object range, r, taken as the perpendicular distance from the plane to the origin of the sensor system, O, is

$$r = \frac{\hat{r}_{11}}{2} + \frac{d\sin\alpha}{2} - \frac{1}{3}\frac{\sqrt{3}d\sin\beta\cos\alpha}{2} \tag{II-3}$$

(b) 2D Type I corner

In the case of a 2D Type I corner, the angle β has been determined already in Section 6 of part I and is the same as the angle ρ in equation (I-35) and Figure I-12. The object range is the distance of the line that passes through the sensor system origin and which is perpendicular to the surface intersection of the 2D corner. Using the cosine rule on triangle $T1$-C-O in Figure II-2,

$$r^2 = \frac{\hat{r}_{11}^2 + d^2}{4} + \frac{d^2\sin^2\beta}{12} - \frac{d\hat{r}_{11}}{2\sqrt{3}}\sin\beta\cos\theta_{11} + \frac{d\hat{r}_{11}}{2}\sin\theta_{11} \tag{II-4}$$

where the value of θ_{11} is given in equation (I-9). The angle γ is expressed as

$$\gamma = \cos^{-1}\left(\frac{r^2 + c^2 - \hat{r}_{11}^2/4}{2cr}\right) \tag{II-5}$$

* This work was conducted at the Dept. of Electrical and Computer Systems Engineering, Monash University, Clayton, Australia under the Monash Graduate Scholarship. Part I appeared in the previous issue of *Robotica.*

** School of Applied Science, Nanyang Technological University (Singapore).

† Intelligent Robotics Research Centre Department of Electrical and Computer Systems Engineering, Monash University, Clayton, Victoria 3168 (Australia).

https://doi.org/10.1017/S0263574797000775 Published online by Cambridge University Press

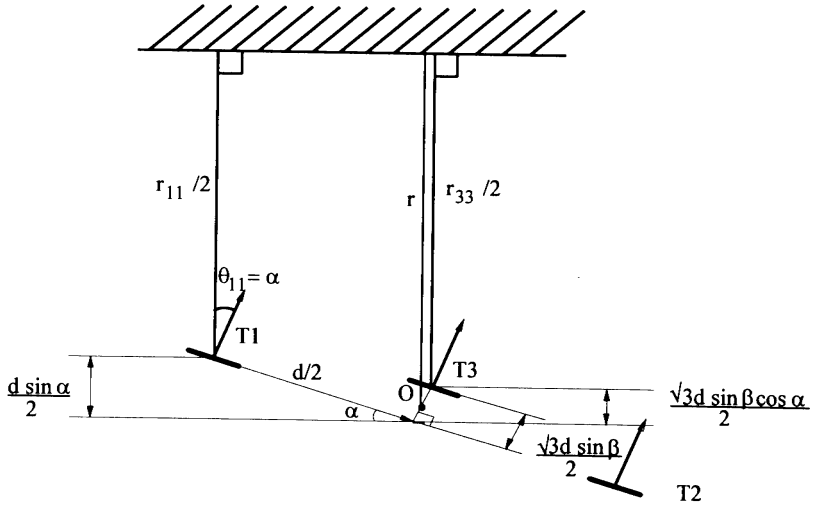

Fig. II-1. Illustration showing angle and distance relationships between $T1$ and $T3$ for a plane.

where

$$c^2 = \frac{d^2}{4} + \frac{d^2 \sin^2 \beta}{12} \tag{II-6}$$

and α is given by

$$\alpha = \pi - \gamma - \cos^{-1}\left(\frac{d \sin \beta}{2c\sqrt{3}}\right) \tag{II-7}$$

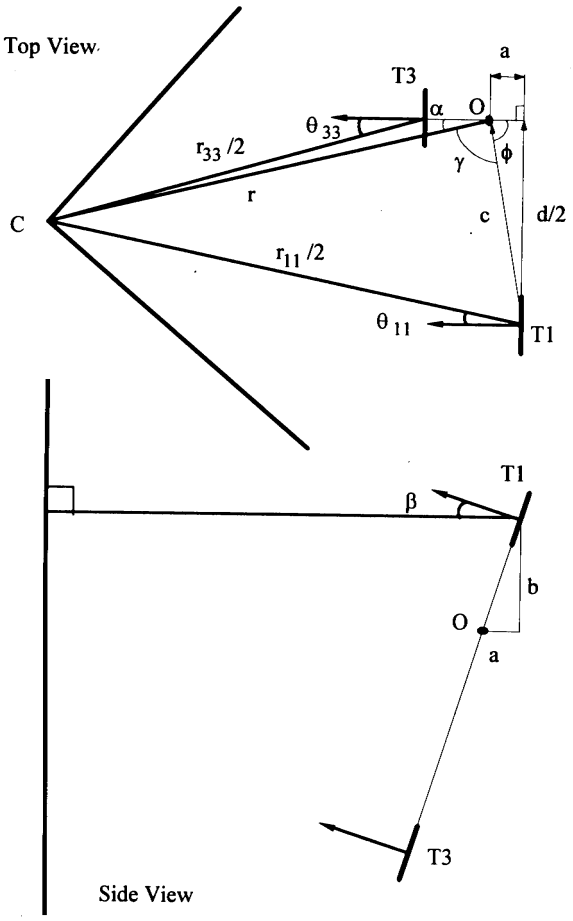

Fig. II-2. Illustration showing angle and distance relationships between $T1$, $T3$ and sensor origin O for a 2D Type I corner.

(c) 2D Type II corner type

The aximuth α illustrated in Figure II-3 is the same as the angle ρ in equation (I-10) and Figure I-10. The values of a and ϕ are as shown below:

$$a^2 = \left(\frac{d \sin \alpha}{2}\right)^2 + \left(\frac{\sqrt{3}\, d}{2 \times 3}\right)^2,$$
$$\sin \phi = \frac{\sqrt{3}\, d}{2 \times 3a}, \quad \cos \phi = \frac{d \sin \alpha}{2a}. \tag{II-8}$$

The object range r is derived using the cosine rule for triangle $T1$-O-V:

$$r^2 = \frac{\hat{r}_{11}^2}{4} + a^2 + a\hat{r}_{11} \cos(\phi - \theta_{11})$$
$$= \frac{3\hat{r}_{11}^2 + d^2}{12} + \frac{d^2 \sin^2 \alpha}{4} + \frac{d\hat{r}_{11}}{2} \sin \alpha \cos \theta_{11} + \frac{d\hat{r}_{11}}{2\sqrt{3}} \sin \theta_{11} \tag{II-9}$$

where

$$\theta_{11} = \sin^{-1}\left(\frac{2r_{33}^2 - r_{11}^2 - r_{22}^2 - 6d^2 + 3(r_{22} - r_{11})^2}{4\sqrt{3} d r_{11}}\right) \tag{II-10}$$

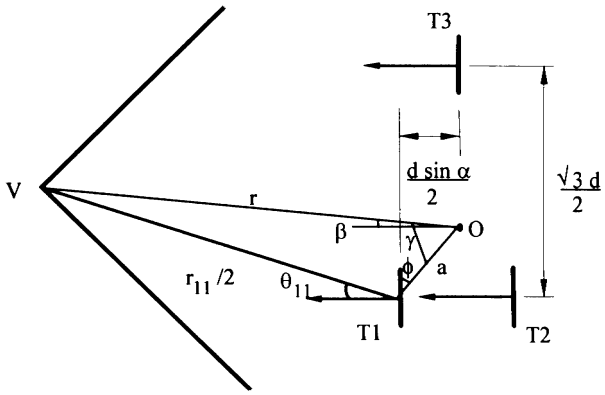

Fig. II-3. Illustration showing derivation of object distance and rotational angle about v axis for 2D Type II corner.

https://doi.org/10.1017/S0263574797000775 Published online by Cambridge University Press

The elevation β can be represented by

$$\beta = \pi - \gamma + \cos^{-1}\left(\frac{d \sin \alpha}{2a}\right) \tag{II-11}$$

where

$$\gamma = \cos^{-1}\left(\frac{r^2 + a^2 - \hat{r}_{11}^2/4}{2ar}\right) \tag{II-12}$$

(d) 3D corner

In Section 3 of part I, the virtual images of the two transducers over a 3D corner are shown to be the same as those over an appropriately aligned 2D corner. For this analysis, the three transducers are thus considered in *pairs.* The object range is the distance from the corner vertex, *V,* to the system origin, *O*. However, it is necessary to consider the third transducer in order to determine the azimuth, elevation and object range. From Figure II-4,

$$\frac{r_{33}^2}{4} = \frac{r_{33}'^2}{4} + \frac{3d^2}{4}\cos^2 \rho \tag{II-13}$$

and

$$\begin{aligned} r_{33}' \cos \theta_{33} &= r_{11} \cos \theta_{11} - \sqrt{3} d \sin \rho \\ r_{33}' \sin \theta_{33} &= r_{11} \sin \theta_{11} + d \end{aligned} \tag{II-14}$$

gives

$$\rho = \sin^{-1}\left(\frac{\hat{r}_{11}^2 + 4d^2 + 2d\hat{r}_{11} \sin \theta_{11} - \hat{r}_{33}^2}{2\sqrt{3} d \hat{r}_{11} \cos \theta_{11}}\right) \tag{II-15}$$

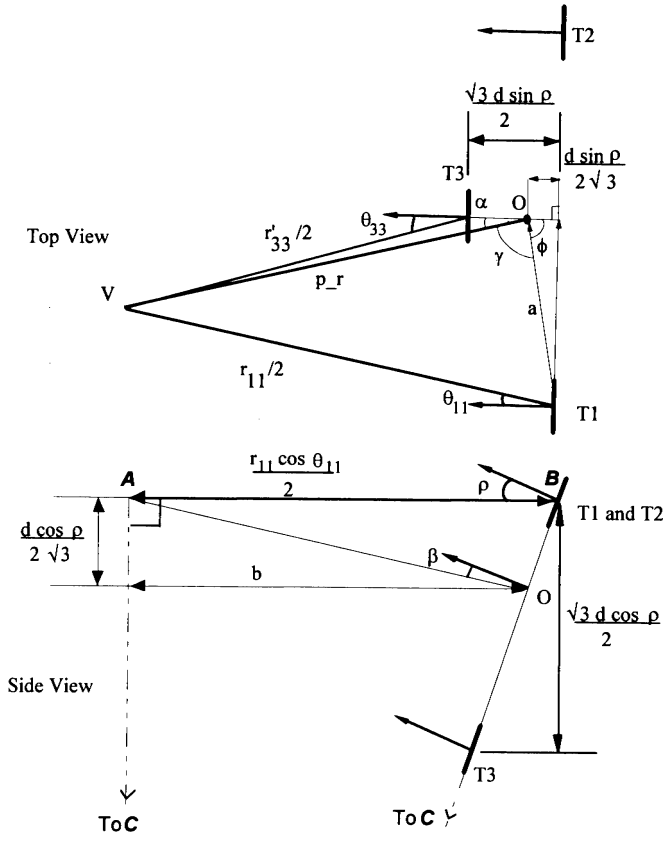

Fig. II-4. Illustration showing angle and distance relationships between *T*1, *T*3 and sensor origin *O* for a 3D corner.

where θ_{11} is derived in the same manner as that for equation (I-31):

$$\theta_{11} = \sin^{-1}\left(\frac{r_{22}^2 - r_{11}^2 - 4d^2}{4r_{11}d}\right) \tag{II-16}$$

The top projection of the object range, p_r, can be expressed in a similar manner to equation (II-9),

$$\begin{aligned} p\_r^2 &= \frac{\hat{r}_{11}^2}{4} + a^2 - \hat{r}_{11} a \cos(\theta_{11} + \phi) \\ &= \frac{\hat{r}_{11}^2 + d^2}{4} + \frac{d^2 \sin^2 \rho}{12} - \frac{d\hat{r}_{11}}{2\sqrt{3}} \sin \rho \cos \theta_{11} + \frac{d\hat{r}_{11}}{2} \sin \theta_{11} \end{aligned} \tag{II-17}$$

where

$$a^2 = \frac{d^2}{4} + \frac{d^2}{12}\sin^2 \rho \tag{II-18}$$

$$\cos \phi = \frac{d \sin \rho}{2a\sqrt{3}}, \quad \sin \phi = \frac{d}{2a} \tag{II-19}$$

and

$$\alpha = \pi - \cos^{-1}\left(\frac{p\_r^2 + a^2 - \hat{r}_{11}^2/4}{2ap\_r}\right) - \cos^{-1}\left(\frac{d \sin \rho}{2\sqrt{3}a}\right) \tag{II-20}$$

The object range is then easily obtained by taking into account the projection depth,

$$r^2 = p\_r^2 + \frac{d^2}{12}\cos^2 \rho \tag{II-21}$$

The angle ρ in this case is not equal to the elevation β as β is measured with respect to the normal of the sensor system positioned at its origin. The solution to finding β becomes quite simple if the side view is modified such that a right angle triangle **ABC** is formed as shown in Figure II-4. The height of this triangle h is

$$h = \frac{\hat{r}_{11} \cos \theta_{11}}{2 \tan \rho} \tag{II-22}$$

Using the method of similar triangles, the distance b can be expressed as

$$b = \frac{\hat{r}_{11}}{2} \cos \theta_{11} \times \frac{h - (d \cos \rho)/(2\sqrt{3})}{h} \tag{II-23}$$

The angle β is thus

$$\beta = \rho - \tan^{-1}\left(\frac{d \cos \rho}{2\sqrt{3} b}\right) \tag{II-24}$$

2. SENSOR SYSTEM IMPLEMENTATION

(a) Polaroid transducer

The Polaroid instrument grade ultrasonic transducer is employed in the sensor design. It is an electrostatic transducer and operates as a transmitter similar to a diaphragm loudspeaker and a receiver similar to a capacitor microphone. Its frequency response is superior to those of piezoelectric devices. The beam pattern of the Polaroid transducer is a good approximation to a

https://doi.org/10.1017/S0263574797000775 Published online by Cambridge University Press

Gaussian distribution with a half-angle, θ_0 of about 12° as in equation (II-25). A custom designed electronic circuit supplied by 300 V DC is used to generate transmission pulses for the Polaroid transducers and measure received echoes. The transmit signal is 16 cycles of a square wave at 49.4 kHz.

(b) Operating range

Three Polaroid ultrasonic transducers are arranged in an equilateral triangle with an inter-transducer spacing d of 200 mm. The value of d was chosen by considering its effect on the system's performance at short and long object ranges. If the reflector is a plane at close range, a large value of d will result in small signal amplitudes received at $T2$ from transmitter $T1'$, at $T1$ from transmitter $T2'$, and so on. Thus the maximum value of d is governed by the minimum desired signal amplitude at the minimum object range. In the case of a Polaroid transducer, the beam pattern follows a Gaussian approximation[13] and the amplitude of an echo received, not considering any energy losses, in a configuration shown in Figure II-5 can be approximated by,

$$\text{echo amplitude} \propto \exp\left[\frac{-2(\theta^2_{\text{reflectance}} + \theta^2_{\text{incidence}})}{\theta_0^2}\right] = \exp\left[\frac{-4\theta^2}{\theta_0^2}\right] \quad \text{(II-25)}$$

where θ_0 is the beam angle which is measured to be 12°.

If the ratio of the minimum and maximum amplitudes is p and the minimum object range is $r_{\min}$,

$$d \leq 2r_{\min} \tan\left(\sqrt{\frac{\theta_0^2 \ln p}{-4}}\right) \quad (26)$$

When the object range is large compared to d, the relative difference in distances of flight between transmitters and receivers is small. This is true for all the four classes of reflectors. This method no longer works satisfactorily when these differences are comparable to the errors in measurements. In practice, the value of d is thus set to its allowable maximum. If p is 0.2 and the minimum object distance $r_{\min}$ is 0.75 m, the maximum inter-transducer spacing is therefore 205 mm. The inter-transducer spacing d used in this research is 200 mm. The assumption of parallelism outlined in Section VI(c) for 2D Type II Corner in Part I is also valid, because $d \sin\theta_0 = 0.04$ m which is small compared to the minimum object distance of 0.75 m.

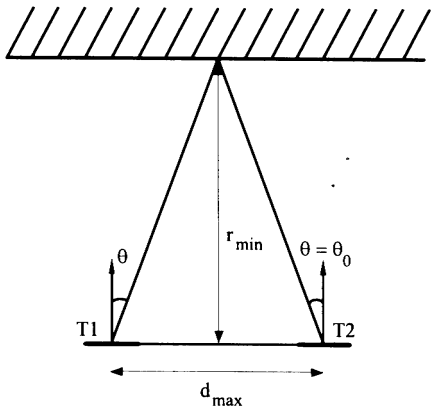

Fig. II-5. Relationship between the minimum object distance $r_{\min}$ and the maximum inter-transducer spacing d.

(c) Time of flight measurement

A simple technique has been chosen to measure the time of flight. It uses the time axis intercept of the linear fit of the first two sampled data corresponding to the echo's leading edge. The time measurement error is within 1 μs for distances of flight between 1.5 m and 6 m after adjustment for systematic errors such as timer activation delays.

3. EXPERIMENTAL RESULTS OF THE MLE TECHNIQUE

A model of a 0.75 m × 0.75 m × 0.75 m 3D corner was fabricated using strengthened plywood. The planes and 2D corner of this model were used as test reflectors also.

(a) Reflector classification

After the application of MLE, the unitless minimised least-squares errors in equation (I-33), S, are used to determine which reflector class a test object belongs to. As a result, the values of S are presented here to illustrate the success of the method. There are four reflector classes namely (1) plane, (2) 2D Type I corner, (3) 2D Type II corner and (4) 3D corner. Two hundred samples were taken for each data point. The threshold corresponding to 95% confidence level with six degrees of freedom (12.6) was used as discussed in Section 7 of part I.

Table II-1 shows the average values of S for various reflectors tested against the four test classes. The actual reflectors tested are marked with an asterisk (*) in the column for Test Classes. When the test classes correspond to the actual reflectors, the S values are found to be less than the threshold of 12.6. For incorrect matches, the S values are far greater than this threshold.

Table II-1. Average values of S for different objects and test classes.

Test Class	Object Distance (m)							
	0.75	1.00	1.25	1.50	1.75	2.00	2.25	2.50
plane*	2.1	1.4	2.5	1.0	1.3	1.4	1.2	2.3
2Dc I	448.8	290.9	194.0	131.2	97.1	72.7	60.6	48.5
2Dc II	654.3	351.3	242.4	155.2	121.2	89.7	77.6	72.7
3Dc	1054.5	581.8	400.1	254.5	193.9	140.6	123.1	109.1
plane	549.8	325.5	221.9	146.3	132.6	108.4	76.1	—
2Dc I*	2.1	2.0	2.5	1.3	4.3	5.0	2.7	—
2Dc II	1279.5	747.0	498.2	309.6	273.5	214.2	167.3	—
3Dc	670.0	404.1	266.4	156.1	139.0	106.0	90.1	—
plane	566.8	363.0	235.7	146.3	97	87.5	50.9	41.6
2Dc I	1140.6	718.1	453.5	297.1	203.0	163.8	113.7	87.9
2Dc II*	5.3	1.9	3.3	2.0	3.6	1.5	3.5	3.5
3Dc	540.7	336.3	208.3	144.1	103.3	73.0	62.4	46.7
plane	—	685.5	384.1	276.6	194	169.1	101.4	—
2Dc I	—	403.2	245.2	166.4	120.9	111.1	65.9	—
2Dc II	—	304.6	156.2	121.1	82.3	66.2	47.7	—
3Dc*	—	3.7	5.2	2.6	3.0	3.5	8.4	—

https://doi.org/10.1017/S0263574797000775 Published online by Cambridge University Press

The margin between the S values for correct and incorrect class matches is large. As a result, successful 3D reflector identifications can be achieved. However, the S values for incorrect matches decrease with increasing object distance while the S for the correct match increases. This is because the relative differences between the echo times of flight become smaller as the object distance increases. One solution to this operating range limitation is to introduce variable inter-transducer spacing.

(b) Object localisation

This technique is found to produce good accuracy in spite of the simple hardware used in processing the received signals. Range accuracy to within 2 mm is achieved. The angular errors (measured minus actual) are plotted in Figures II-6 and II-7. It was found that the system is less accurate at larger rotational angles. This is due to the small echoes received which make measurements of the arrival times less accurate. In most cases, angular accuracy of at least 0.5° can be achieved.

(c) Discussion

This method uses ultrasonic signals and relies on specular reflection to provide unique signal echo paths when the signals are directed at planes, 2D corners and 3D corners. As a result, it suffers from the poor reflectivity of certain object surfaces (such carpets, curtains, and cardboard) which absorb and diffuse ultrasonic waves. However, as long as the reflected echoes are not too weak to be detected, the noise standard deviation of the range measurements in the MLE can be set to accommodate the resultant measurement errors. There are also time of flight measuring techniques such as the matched filter method used by Kleeman Kuc[10] which can measure accurately arrival times of weak specular echoes. The current MLE target identification and localisation algorithm is fast requiring 70 ms processing time on a 40 MHz Intel 386 with coprocessor.

4. IMPLEMENTATION ON A MOBILE ROBOT

The sensor system was applied to a real robot localisation problem to demonstrate its practicality and robustness. An *a priori* model of the environment consisting of the types and locations of full 3D navigation beacons was measured using a tape.

The robot localisation algorithm used in this experiment is based on that developed by Durrant-Whyte and Leonard[3,20,21] which integrates odometry with other sensory data from geometric beacons. This method was selected because firstly, it uses an *a priori* environment model; secondly, it can be easily adapted to include planes, 2D and 3D corners as geometrical beacons; and thirdly, the Extended Kalman Filter employed possesses simplicity and elegance in the integration of sensory information, system dynamics and statistical uncertainties and the generation of the uncertainty associated with each estimate.[22]

The experiment was conducted on a Fander robot. Communication between an IBM AT 286 Compatible and the robot is established via an RS-232 serial link. Figure II-8 shows the plan of a laboratory used as the test environment. The environment was modified to conceal the doorway and other equipment. The modification also introduced the need for membership testing as described later.

The problem was designed to be testing as follows: Firstly, the worst case indoor scenario is assumed in the sense that all walls (planes) and wall-wall 2D corners were concealed and the robot could only use floor-wall (ceiling-wall) 2D and 3D corners. The floor-wall intersections and corners were used in this demonstration because the robot is only 35 cm in height. Secondly, the path of the robot is rectangular, requiring the robot to continuously make right-angle turns followed by straight line movements of over 1 metre. These manoeuvres are usually associated with large odometric errors. Thirdly, the walls and corners in the environment were not perfectly flat or exactly at right angles, but with a tolerance about ±1°.

(a) Robot localisation

The motion taken by the robot is shown in Table II-2. The initial position of the robot is destination 0, and the robot moves around the room following the destination sequence 1, 2, 3, 4, 1, . . . , 4, 1, etc. The heading angle is measured with respect to the X axis anticlockwise. At every stop, the position of the robot is predicted using its previous position and odometry.

The predicted state equation $\hat{\mathbf{x}}(k+1 \mid k)$ for the robot position is

$$\hat{\mathbf{x}}(k+1 \mid k) = \mathbf{f}[\hat{\mathbf{x}}(k \mid k), \mathbf{u}(k)] = \begin{bmatrix} \hat{x}_R(k \mid k) + D(k) \sin \hat{\theta}_R(k \mid k) \\ \hat{y}_R(k \mid k) + D(k) \cos \hat{\theta}_R(k \mid k) \\ \hat{\theta}_R(k \mid k) + \Delta\theta_R(k) \end{bmatrix} \quad \text{(II-27)}$$

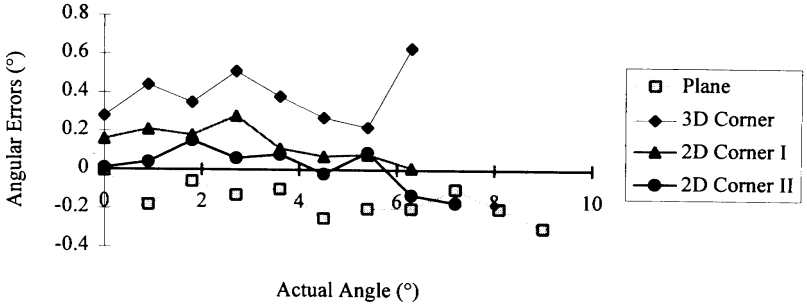

Fig. II-6. Angular error against actual rotational angles about u axis at 1.5 m.

https://doi.org/10.1017/S0263574797000775 Published online by Cambridge University Press

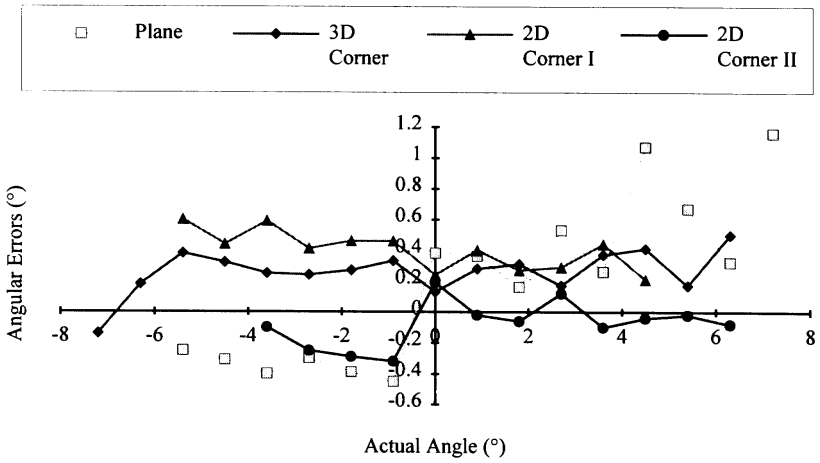

Fig. II-7. Angular errors against actual angles about v axis at 1.5 m.

when the robot moves a distance $D(k)$ and rotates an angle $\Delta\theta_R(k)$ at time $k+1$ as shown in Figure II-9.

Based on the current predicted robot location, the predicted locations of all navigation beacons in the environment are obtained by transforming the *a priori* environment model to the robot frame. Each predicted beacon location is represented by the azimuth α, elevation β, and range r. The observation matrix is

$$\mathbf{h}[k+1, \hat{\mathbf{x}}(k+1 \mid k)] = \begin{bmatrix} \hat{r}(k+1) \\ \hat{\alpha}(k+1) \end{bmatrix} \qquad \text{(II-28)}$$

The elevation β is not used because the floor is assumed to be level. However, its inclusion is straight forward.

When a valid object is found at a beacon location, it is tested for validity by its *type* and *membership*. This is a variation of the technique adopted by Durrant-Whyte and Leonard[3,20] which only uses membership tests.

The purpose of the type test is to eliminate all improbable beacon matches at the earliest opportunity so that the next beacon on the visibility list can be observed. However, a successful classification test alone is insufficient to ascertain the validity of the beacon. An example is shown in Figure II-10. The robot, in searching for beacon A, encounters beacon B and, as a result of erroneous position prediction, rightly classify it as a 2D corner and wrongly identify it as beacon A. The utility of wrong navigation beacons as references is a serious error which can confuse the localisation algorithm. Such situations can be avoided by a second test of which purpose is to test "*for membership in the validation gate*" g.[3,20] This value g is also known as the Mahalanobis distance in computer vision.[23] If g falls below a threshold, the observation is valid. From the χ^2 tables, a threshold of 9.21 at two degrees of freedom and 99% confidence is selected for this demonstration.

If no object is found at the expected location or the beacon found is not valid, the motorised sensor system is instructed to scan the vicinity of the expected target position with the scan pattern in Figure II-11a. The step size used by both stepper motors is 4.5°. This value was chosen after examination of the experimental results on angle limits (Section X) to ensure some degree of overlapping of view angles at consecutive scan position as sown in Figure II-11b. The search ends when a valid beacon is found or when the scan pattern is completed. The position and orientation of the robot is then estimated using the EKF for every visible beacon.

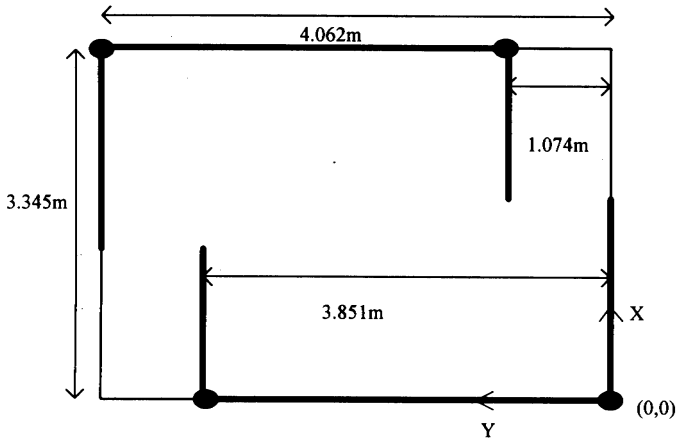

Fig. II-8. Floor plan of environment used in the demonstration. The filled circles and thick boundaries denote the 3D corners and 2D corners which are used as beacons in the demonstration.

(b) Results and discussion

In the first demonstration, the mobile robot vehicle was required to follow the motion sequence mentioned above without using any external beacons for robot localisation. The planning of its motion was based solely on odometry with no position correction. It can be seen, from Figure II-12, that the positional and heading errors of the root grow very quickly without bounds. By the end of the

Table II-2. Desired position of robot in the room.

Destination	X (m)	Y (m)	Heading (°)
0	1.00	1.00	90
1	1.00	2.84	90
2	2.35	2.84	0
3	2.35	2.07	−90
4	1.00	2.07	−180

https://doi.org/10.1017/S0263574797000775 Published online by Cambridge University Press

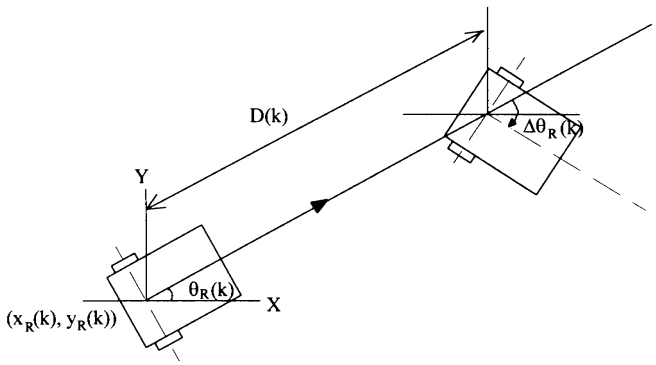

Fig. II-9. Straight line and turn motions of a robot.

demonstration, the position of the robot was out by more than 500 mm in both the X and Y directions, and the error in robot orientation was more than 60°. This experiment is an illustration of the drawback of dead reckoning.

The next demonstration conducted required the mobile robot system to correct for the odeometry errors while going through the same motion sequence as before.

The comparison of the experimental results of localisation in close loop control with measurements by hand and tape is shown in Figures II-13 and II-14. There is apparently a positive bias of about 0.6° in the heading error. This is attributed to a small misalignment in the mechanical structure. The positional error is maintained within 10 mm.

There are, however, some limitations of the current MLE method in robot localisation.

- The working range of the MLE method depends on the inter-transducer spacing d and the technique used to measure echo arrival times. With the current sensor system, the maximum object distance is about 3 metres, limiting the size of the environment the sensor system can operate in. Better time of flight measurement systems[10] and variable inter-transducer spacing can be used to improve the working range.
- This method cannot be applied to environments where there are no well-defined planes and right-angles corners.
- In situations where there are obstructions of these beacons such as electrical wiring or cornices along the ceiling-wall intersection or skirting boards along the floor, this method may fail. Moreover, the echoes reflected off the top surface of the skirting board and from the board-floor intersection may overlap if the distance between the sensor and the skirting board is large.
- Due to the long transmitted pulse used (~320 μs), the desired echoes may not be isolated easily from those of nearby clutter if the echoes overlap. Objects with rough or low reflectivity surfaces may diffuse or absorb the ultrasonic signal, making measurements of the echo arrival times difficult or impossible.

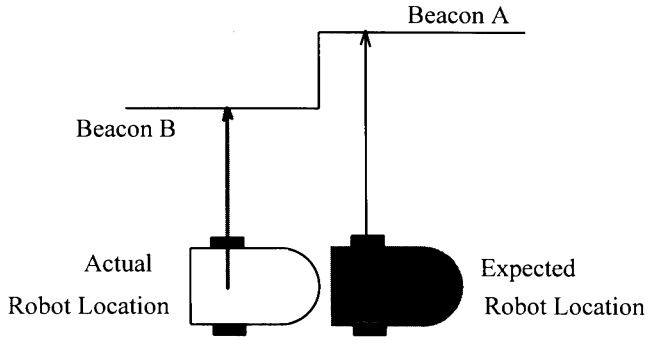

Fig. II-10. An example of possible mistaken beacon identity.

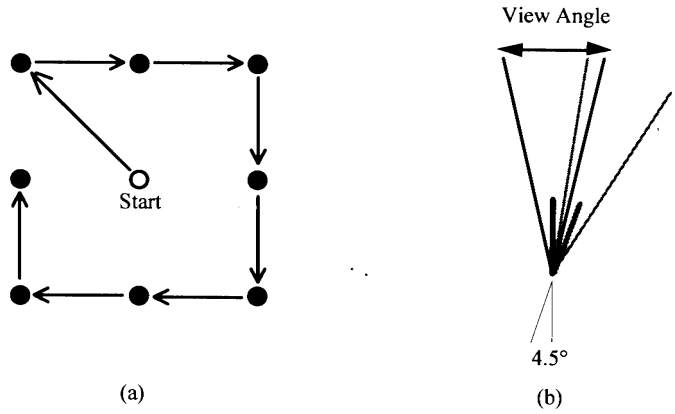

Fig. II-11. (a) Scan pattern of sensor system. (b) Overlapping of view angles between scan positions.

5. CONCLUSION

The research presented in this paper provides additional flexibility to ultrasonic localisation systems by allowing them to identify and locate 3D natural beacons. This enables the sensor system to break away from the 'horizontal scan' constraint. The natural beacons used in this research are planes, 2D and 3D corners which are very common features in most indoor environment.

The method presented can identify and localise 3D geometrical targets with a low sampling rate (59 kHz)

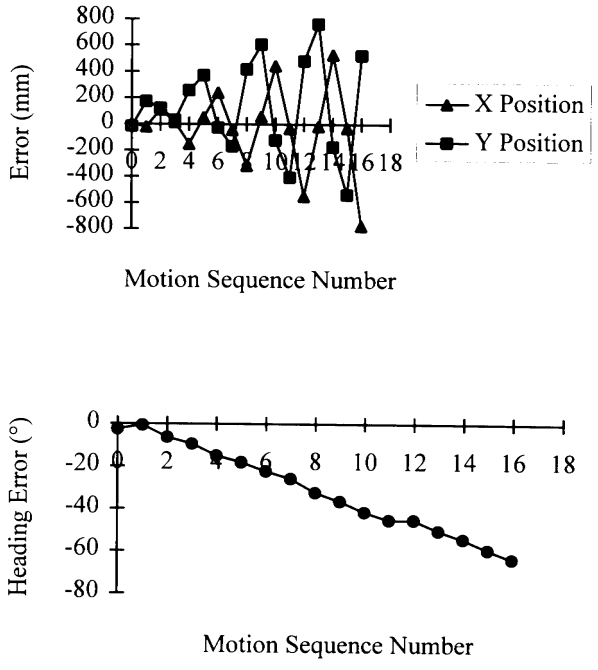

Fig. II-12. Positional and heading errors during robot navigation when only odometry was used.

https://doi.org/10.1017/S0263574797000775 Published online by Cambridge University Press

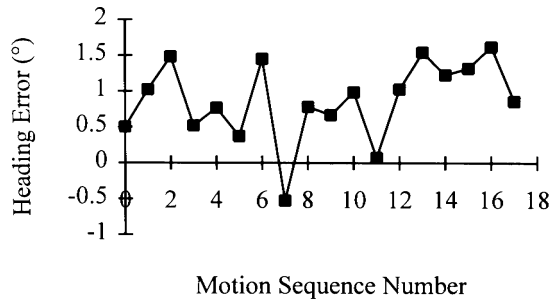

Fig. II-13. Orientation difference between bearing angles obtained from the sensor system and those from hand measurements.

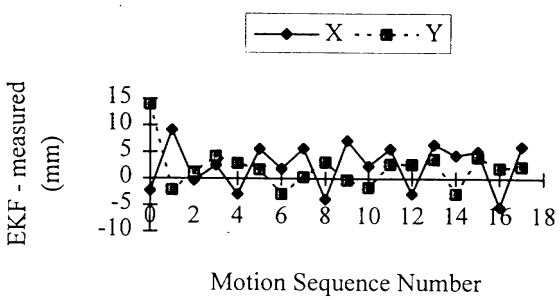

Fig. II-14. Positional differences between data obtained from sensor system and that from hand measurements.

ultrasonic sensor system. The target identification and localisation algorithm requires 70 ms on a 40 MHz Intel 386 with coprocessor. Moreover, the strength of this technique lies in the determination of the *most likely beacon location* based on the measurements and supporting statistical information. The performance of the beacon localisation technique using times of flight and the MLE has been applied and tested on a wheeled mobile robot navigation in an indoor environment. These imperfections in the beacons and the good accuracy (within 10 mm in position and 2° in heading) achieved by the sensor system demonstrate the robustness of the MLE time of flight sensor system used in conjunction with the EKF robot localisation algorithm.

References

1. M. Drumheller, "Mobile robot localization using sonar" *IEEE Transactions on Pattern Analysis and Machine Intelligence* **PAMI-9,** No. 2, 325–332 (1987).
2. J.L. Crowley, "World modeling and position estimation for a mobile robot using ultrasonic ranging" *Proceedings of IEEE International Conference on Robotics and Automation* (1989) pp. 674–680.
3. J.J. Leonard and H.F. Durrnat-Whyte, *Directed Sonar Sensing for Mobile Robot Navigation,* (Kluwer Academic Press, Boston, 1992).
4. L. Kleeman, "Ultrasonic automonous robot localisation system" In *Proceedings of IEEE/RSJ International Workshop on Intelligent Robots and Systems,* Tsukuba, Japan (1989), pp. 212–219.
5. L. Kleeman, "Iterative algorithm for three dimensional autonomous robot localisation" *Proceedings of Third National Conference on Robotics,* Melbourne, Australia (1990) pp. 210–219.
6. L. Kleeman, "A three dimensional localiser for autonomous robot vehicles" *Robotica* **13,** Part 1, 87–94 (1995).
7. J.B. LeMay and J. Lamancusa, "Error minimization and redundancy management for a three dimensional ultrasonic ranging system" *Proceedings of IEEE/RSJ International Conference on Intelligent Robots and Systems,* Raleigh, N.C. (1992) pp. 837–844.
8. A.M. Sabatini, "Active hearing for external imaging based on an ultrasonic transducer array" *Proceedings of 1992 IEEE/RSJ International Conference on Intelligent Robots and Systems,* Raleigh, N.C. (1992) pp. 829–836.
9. H. Peremans, K. Audenaert *et al.,* "A high-resolution sensor based on tri-aural perception" *IEEE Transactions on Robotics and Automation* **9,** No. 1, 36–48 (1993).
10. L. Kleeman and R. Kuc, "Mobile robot sonar for target localization and classification" *Int. J. Robotica Research* **14,** No. 4, 295–318 (August, 1995).
11. J.H. Ko, W.J. Kim *et al.,* "A method of ultrasonic sensor data integration for floorplan recognition" *Proceedings of International Symposium on Intelligent Control,* Chicago, Illonia, USA (1993) pp. 346–351.
12. R. Kuc and Y. Di, "Intelligent sensor approach to differentiating somar reflections from corners and planes" *Proceedings of Internatiionsl Congress on Intelligent Autonomous Systems,* Amsterdam, The Netherlands (1986) pp. 329–333.
13. B. Barshan and R. Kuc, "Differentiating sonar reflections from corners and planes by employing an intelligent sensor" *IEEE Transactions on Pattern Analysis and Machine Intelligence* **12,** No. 6, 560–569 (1990).
14. K. Sasaki and M. Takano, "Classification of objects' surface by acoustic transfer function" *Proceedings of IEEE/RSJ International Conference on Intelligent Robots and Systems,* Rayleigh, N.C. (1992) pp. 821–828.
15. L. Kleeman and R. Kuc, "An optimal sonar array for target localization and classification" *Proceedings of IEEE International Conference on Robotics and Automation,* San Diego USA (1994) pp. 3130–3135.
16. H. Akbarally and L. Kleeman, "A sonar sensor for accurate 3D target localisation and classification" *Proceedings of IEEE International Conference on Robotics and Automation,* Nagoya, Japan (1995) pp. 3003–3008.
17. M.L. Hong and L. Kleeman, "A low sample rate 3D sonar sensor for mobile robots" *Proceedings of IEEE International Conference on Robotics and Automation,* Nagoya, Japan (1995) pp. 3015–3020.
18. A.D. Whalen, *Detection of Signals in Noise* (Academic Press, New York, 1971a).
19. Y. Bar-Shalom and T.E. Fortmann, *Tracking and Data Association* Academic Press, Boston, 1988).
20. J.J. Leonard and H.F. Durrante-Whyte, "Mobile robot localization by tracking geometric beacons" *IEEE Transactions on Robotics and Automation* **7,** No. 3, 376–382 (1991).
21. H.F. Durrant-Whyte and J.J. Leonard, "Navigation by correlating geometric sensor data" *Proceedings of IEEE/RSJ International Workshop on Intelligent Robots and Systems '89*, Tsukuba, Japan (1989) pp. 440–447.
22. M.L. Hong, "Three-dimensional ultrasonic sensing for autonomous vehicles", *PhD Thesis* (Monash University, February 1995).
23. N. Ayache and O.D. Faugeras, "Maintaining representations of the environment of a mobile robot" *IEEE Transactions on Robotics and Automation* **5,** No. 6, 804–819 (1989).

https://doi.org/10.1017/S0263574797000775 Published online by Cambridge University Press